Simulation of transonic flutter and active shockwave control

L. Djayapertapa and C.B. Allen
Department of Aerospace Engineering, University of Bristol, Bristol, Avon, UK

Keywords *Elasticity, Flight control, Flight dynamics, Aerodynamics*

Received August 2001
Revised August 2002
Accepted October 2002

Abstract *Transonic flutter and active flap control, in two dimensions, are simulated by coupling independent structural dynamic and inviscid aerodynamic models, in the time domain. A flight control system, to actively control the trailing edge flap motion, has also been incorporated and, since this requires perfect synchronisation of fluid, structure and control signal, the "strong" coupling approach is adopted. The computational method developed is used to perform transonic aeroelastic and aeroservoelastic calculations in the time domain, and used to compute stability (flutter) boundaries of 2D wing sections. Open and closed loop simulations show that active control can successfully suppress flutter and results in a significant increase in the allowable speed index in the transonic regime. It is also shown that active control is still effective when there is free-play in the control surface hinge. Flowfield analysis is used to investigate the nature of flutter and active control, and the fundamental importance of shock wave motion in the vicinity of the flap is demonstrated.*

Nomenclature

a_∞ = freestream speed of sound
a_h = non-dimensional distance of the elastic axis from midchord, positive aft of midchord
ACT = active control technology
b = aerofoil semi-chord
c = $2b$, aerofoil chord
c_β = non-dimensional distance of hinge axis from midchord, positive aft of midchord
CHM = control hinge moment, non-dimensional
C_L = lift coefficient
C_D = drag coefficient
$C_{M_{ea}}$ = pitching moment coefficient about the elastic axis
e = total specific energy
EA = elastic axis
$\mathbf{F}$ = convective aerodynamic flux
$\mathbf{f_a}$ = non-dimensional aerodynamic loads
$\mathbf{f_c}$ = non-dimensional active control force
$\mathbf{f_{fp}}$ = non-dimensional free-play force
FPM = free-play moment about EA, non-dimensional
FPHM = free-play hinge moment about hinge axis, non-dimensional
G = control law gains
h = plunging displacement (measured +ve downwards)
HA = hinge axis
I_α = polar moment of inertia of aerofoil mass about EA
I_β = polar moment of inertia of control surface mass about EA
$[\mathbf{K}]$ = non-dimensional stiffness matrix
K_h = $m\omega_h^2$, bending stiffness corresponding to plunging displacement
K_α = $I_\alpha\omega_\alpha^2$, torsional stiffness corresponding to pitching rotation
K_β = $I_\beta\omega_\beta^2$, torsional stiffness corresponding to control surface rotation
L = $q_\infty c C_L$, aerodynamic lift

The authors would like to acknowledge the contribution of Professor S.P. Fiddes, who originally supervised Mr Djayapertapa's PhD research, to this work.

International Journal of Numerical Methods for Heat & Fluid Flow
Vol. 14 No. 4, 2004
pp. 413-443

0961-5539
DOI 10.1108/09615530410532231

LCO = limit cycle oscillations
m = mass of the aerofoil per unit span
$[\mathbf{M}]$ = non-dimensional mass matrix
M_∞ = free-stream Mach number
M_{ea} = $q_\infty c^2 C_{M_{ea}}$ pitching moment about elastic axis (EA)
$\mathbf{n}$ = cell face outward unit normal
q_∞ = $1/2\rho_\infty U_\infty^2$, free-stream dynamic pressure
r_α = I_α/mb^2, aerofoil radius of gyration about EA in semi-chords, non-dimensional
r_β = I_β/mb^2, control surface radius of gyration about HA in semi-chords, non-dimensional
$\mathbf{R}$ = residual vector
$\mathbf{U}$ = vector of conserved variables
$\mathbf{u}$ = velocity vector
S_α = aerofoil static moment about **EA**
S_β = control surface static moment about hinge axis
t = real time
u, v = cartesian velocity components
$\mathbf{q}$ = structural displacement vector
U_∞ = free-stream velocity
U^* = $U_\infty/\omega_\alpha\sqrt[3]{\mu}$ speed index
V = volume of cell
x, y = cartesian coordinates
x_t, y_t = grid cartesian velocity
$\mathbf{X_t}$ = grid velocity vector
x_α = off-set distance of the aerofoil centre of gravity (CG) from EA, positive aft of EA
x_β = off-set distance of the control surface centre of gravity (CG) from HA, positive aft of HA
α = pitching displacement (positive nose-up)
γ = ratio of specific heats
ρ = density
μ = $m/\pi\rho b^2$, aerofoil-air mass ratio
ξ = h/b, non-dimensional plunging displacement
ω_h = K_h/m, uncoupled plunging natural frequency
ω_α = K_α/I_α, uncoupled pitching natural frequency
ω_β = $K_\beta I_\beta$, uncoupled control surface rotation natural frequency
τ = fictitious pseudo time

1. Introduction

The design cruising speed of civil aircraft often falls within the transonic region, where the structural loads, and hence aeroelastic behaviour, are greatly affected by the presence and motion of shock waves. Hence, the accurate prediction of flutter characteristics of aerofoils in transonic flow is a critical design consideration for most modern civil and high performance aircraft.

In the pure subsonic or supersonic regimes, it has been a normal industry practice to use linear aerodynamic theory, such that the aerodynamic forces depend upon the body motion in linear fashion, thus permitting uncoupling of the structural and fluid equations (MacNeal Schwendler Corporation, 1995). However, this cannot be applied in the transonic regime due to the high non-linearity of the flow field. The aerofoil thickness was often neglected in linear theory, but the aerofoil geometry plays an important role in the development and motion of shock waves in the transonic region (Bland and Edwards, 1984). There are other non-linear phenomena associated with aeroelastics, for example, aileron buzz or limit cycle oscillations (LCO), and none of these phenomena can be predicted directly by traditional linear theoretical methods, since they are interactions between non-linear aerodynamic forces and structures. Hence, more advanced aeroelastic simulation methods, applicable to transonic flows, are essential.

Computational aeroelastics (and aeroservoelastics) often involves two computational models, namely independent aerodynamic and structural

models. In the former, the aircraft surface and the surrounding flow field are discretised, before the governing fluid flow equations are solved. The latter involves solving the structural equations with aerodynamic forces as source terms. (For aeroservoelastics a flight control system is also required.) Coupling these two models in the time domain allows time-accurate simulation of aeroelastic response, and the possibility of identifying flutter boundaries.

It is possible, with current computational power, to develop coupled aerodynamic-structural dynamic methods using the Euler and Navier-Stokes equations as the aerodynamic model. Earlier, euler solvers have been coupled with structural models (Alonso and Jameson, 1994; Bendiksen and Kousen, 1987; Guruswamy, 1990; Kousen and Bendiksen, 1988, 1994; Robinson *et al.*, 1991). The Navier-Stokes equations are still rarely used in computational transonic aeroelasticity mainly due to their excessive CPU demands. Simplified forms of the Navier-Stokes equations have been used for aeroelastic applications (Badcock *et al.*, 1995; Meijer *et al.*, 1998; Prananta and Hounjet, 1996; Prananta *et al.*, 1995; Schuster *et al.*, 1998), but results show that for two degrees of freedom aerofoil motions, little difference was found between using inviscid and viscous aerodynamic models. Reviews of computational aeroelasticity are presented in Bennett and Edwards (1998) and Försching (1995).

The time-accurate interaction between structural dynamics, the flight control system and aerodynamics, known as aeroservoelasticity, has recently received attention, (Batina and Yang, 1984; Edwards *et al.*, 1978; Guillot and Friedman, 1994, 1995; Guruswamy, 1989a, Guruswamy and Tu, 1989b; Horikawa and Dowell, 1979; Karpel, 1982; Nissim, 1971, 1977, 1990; Nissim and Abel, 1978; Nissim *et al.*, 1978; Noll, 1993; Pak *et al.*, 1991; Whalley and Ebrahimi, 1998). Active control technology (ACT) can be implemented within an aeroelastic solver in order to simulate any of the following: flutter suppression, gust alleviation or manoeuver enhancement. Earlier work has relied mainly on transonic small disturbance theory as the aerodynamic solver (Batina and Yang, 1984; Guruswamy, 1989a; Guruswamy and Tu, 1989b) or has been performed in the frequency domain (Batina and Yang, 1984; Edwards *et al.*, 1978; Guillot and Friedman, 1994, 1995; Guruswamy, 1989a, Guruswamy and Tu, 1989b; Horikawa and Dowell, 1979; Karpel, 1982; Nissim, 1990; Pak *et al.*, 1991; Whalley and Ebrahimi, 1998). For example, Nissim (1990, 1971) performed flutter boundary calculations in the frequency domain by considering the sign of the work done by the structural system on its surroundings. There are limitations to this approach, but the energy analysis is extremely useful and is used here.

Active control systems normally have constant (with time) control laws. However, the use of adaptive control in active flutter suppression has started to appear in the literature (Guillot and Friedman, 1994, 1995; Pak *et al.*, 1991). This approach is attractive since the parameters of the system often change with

time or under load, which are the usual limitations of control using fixed-structures and fixed-parameter controllers. The added complexity of adaptive control is often justified by reduced hardware requirements, but it is very difficult to prove the stability properties of controllers whose parameters can vary. In addition, it is almost impossible to get certification for civil aircraft equipped with adaptive control. Hence, the approach of using fixed-parameter controllers is preferred in this research, although it should also be noted that fixed-parameter active controllers are also difficult to certify.

This paper presents a computational method to simulate the aeroelastic and aeroservoelastic behaviour of a two and three degrees of freedom aerofoil. The motions considered are plunge, pitch and control surface (flap) rotation about the hinge axis. The aerodynamic model is described by the Euler equations, which is coupled with a structural model in the time domain, using the "strong" coupling approach. A control law is implemented within the aeroelastic solver to investigate the active means of flutter suppression via control surface (flap) motion, and the effect on the stability (flutter) boundary presented. The mechanics of flutter are examined by considering the phase difference between the plunge and pitch motions for a two degree of freedom model. Transonic flutter is examined using the time-dependent flowfield plots, to demonstrate the effect of active control on shock motion. The effects of free-play in the control surface hinge are also considered.

2. Structural model

Figure 1 shows the typical wing section used to derive the structural equations of motion. This model has been well established for two-dimensional aeroelastic analysis (Dowell *et al.*, 1994; Fung, 1955; Glaser, 1987). The degrees of freedom associated with the aerofoil are shown in Figure 1. The pitching and plunging displacements are restrained by a pair of springs attached to the elastic axis (EA) with spring constants K_α and K_h, respectively. A torsional spring is also attached at the hinge axis whose spring constant is K_β.

Djayapertapa (2001) and Scanlan and Rosenbaum (1951) describe the derivation of the two degrees of freedom aeroelastic equation of motion from Lagrange's equation, and the same principal can be applied to a three degree of freedom system. The resulting governing equations are given by:

$$m\ddot{h} + S_\alpha b\ddot{\alpha} + S_\beta b\ddot{\beta} + K_h h = -L \tag{1}$$

$$S_\alpha b\ddot{h} + I_\alpha\ddot{\alpha} + [(C_\beta - a_h)bS_\beta + I_\beta]\ddot{\beta} + K_\alpha\alpha = M_{\text{ea}} \tag{2}$$

$$S_\beta\ddot{h} + [(C_\beta - a_h)bS_\beta + I_\beta]\ddot{\alpha} + I_\beta\ddot{\beta} + K_\beta\beta = H_\beta \tag{3}$$

where the symbol definitions are shown in Figure 1. S_α is the static moment of the aerofoil about the EA and is given by $S_\alpha = mX_\alpha b$. S_β is the static moment of the control surface about the hinge axis and is given by $S_\beta = mX_\beta b$.

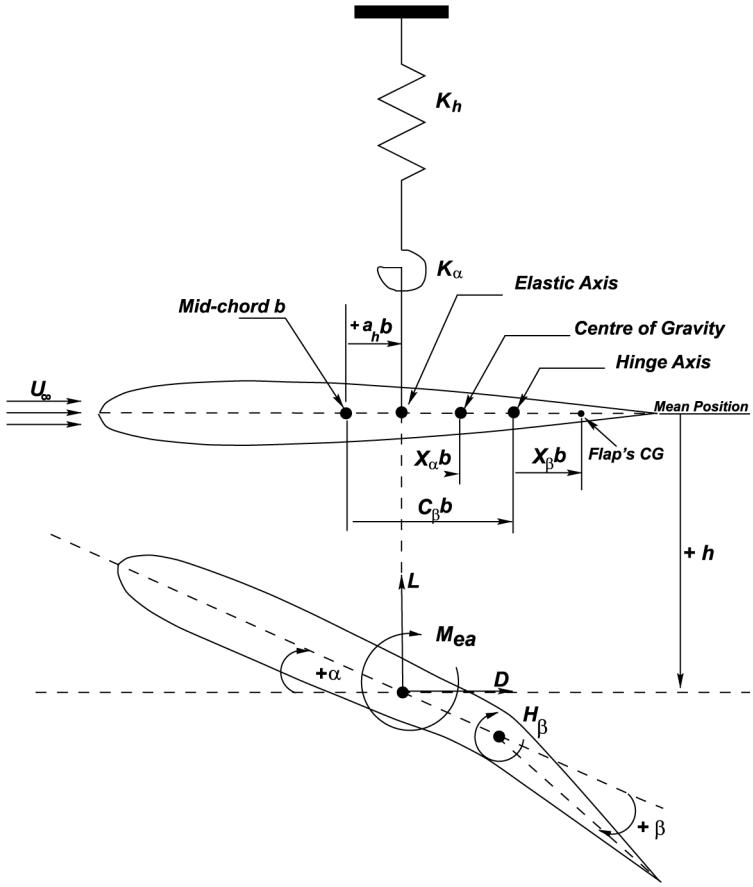

Figure 1.
Aeroelastic parameter definition

$I_\alpha = mr_\alpha^2 b^2$ is the aerofoil moment of inertia about the EA, and $I_\beta = mr_\beta^2 b^2$ is the control surface moment of inertia about the EA.

In order to obtain the full non-dimensional form of the equation, non-dimensional plunge ($\xi = h/b$) and non-dimensional time are introduced. Following the results in the work Djayapertapa (2001), the full non-dimensional form of the aeroelastic equations can be written in the form

$$[\mathbf{M}]\mathbf{q}'' + [\mathbf{K}]\mathbf{q} = \mathbf{f_a} \tag{4}$$

where

$$[\mathbf{M}] = \begin{bmatrix} 1 & x_\alpha & x_\beta \\ x_\alpha & r_\alpha^2 & (C_\beta - a_h)x_\beta + r_\beta^2 \\ x_\beta & (C_\beta - a_h)x_\beta + r_\beta^2 & r_\beta^2 \end{bmatrix} \tag{5}$$

$$[\mathbf{K}] = \frac{4M_\infty^2\gamma}{U^{*2}\mu}\begin{bmatrix} \frac{\omega_h^2}{\omega_\alpha^2} & 0 & 0 \\ 0 & r_\alpha^2 & 0 \\ 0 & 0 & r_\beta^2\frac{\omega_\beta^2}{\omega_\alpha^2} \end{bmatrix}, \tag{6}$$

$$\mathbf{q} = \begin{Bmatrix} \xi \\ \alpha \\ \beta \end{Bmatrix}, \quad \mathbf{f_a} = \frac{4M_\infty^2\gamma}{\pi\mu}\begin{Bmatrix} -C_{\mathrm{L}} \\ 2C_{\mathrm{M_{ea}}} \\ 2C_{\mathrm{H}} \end{Bmatrix} \tag{7}$$

U^* and μ are the non-dimensional speed (the speed index) and mass ratio of aerofoil to air, respectively, and their expressions are given by

$$U^* = \frac{U_\infty}{b\omega_\alpha\sqrt{\mu}}; \qquad \mu = \frac{m}{\pi\rho b^2} \tag{8}$$

2.1 Structural time integration

Equation (4) is solved by approximating it at time level $n+1$, and an implicit Newmark scheme (Bathe, 1982) is used to integrate the equation. Details of the step by step procedure can be found in the work of Djayapertapa (2001).

The choice of time-step in the integration is conditional on accuracy not stability, as the Newmark scheme is unconditionally stable. The size of the time step is governed by the smallest period of the free vibration system (T_{s}). The number of time-steps used per cycle is labelled nspc and so $\Delta t = T_{\mathrm{s}}/\mathrm{nspc}$. The time-step requirements of the Newmark scheme were assessed using a two degree of freedom system, a test case from the works of Bathe (1982). The equations of motion are by

$$\begin{bmatrix} 2.0 & 0.0 \\ 0.0 & 1.0 \end{bmatrix}\begin{Bmatrix} Y_1'' \\ Y_2'' \end{Bmatrix} + \begin{bmatrix} 6.0 & -2.0 \\ -2.0 & 1.0 \end{bmatrix}\begin{Bmatrix} Y_1 \\ Y_2 \end{Bmatrix} = \begin{Bmatrix} 0.0 \\ 10.0 \end{Bmatrix} \tag{9}$$

and the initial conditions are $\mathbf{Y} = \{0,0\}^{\mathrm{T}}$, $\mathbf{Y}' = \{0,0\}^{\mathrm{T}}$. The exact solution of these equations is

$$Y_1 = \frac{5}{3}\left(1 - \cos(\sqrt{2}t)\right) - \frac{2}{3}\left(1 - \cos(\sqrt{5}t)\right) \tag{10}$$

$$Y_2 = \frac{5}{3}\left(1 - \cos(\sqrt{2}t)\right) + \frac{4}{3}\left(1 + \cos(\sqrt{5}t)\right) \tag{11}$$

Figure 2 shows the responses for nspc = 20 and 30. It is clear that 30 time-steps per cycle gives acceptable accuracy, and this is not an excessive number,

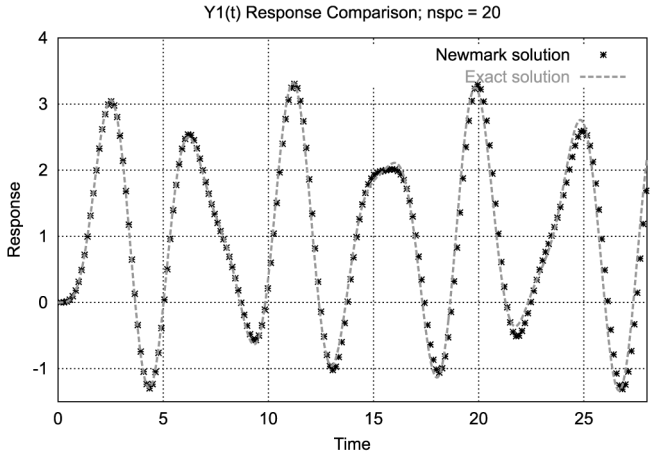

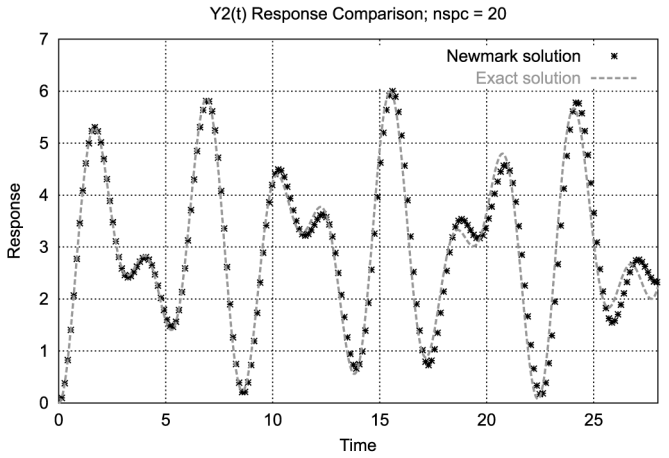

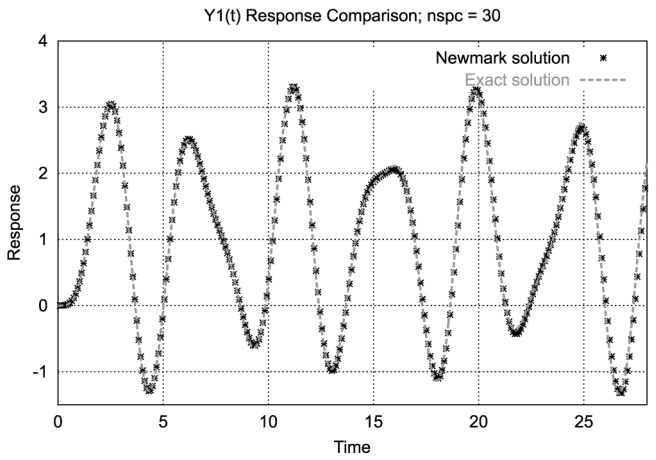

(*continued*)

Figure 2.
Response comparison
Newmark scheme

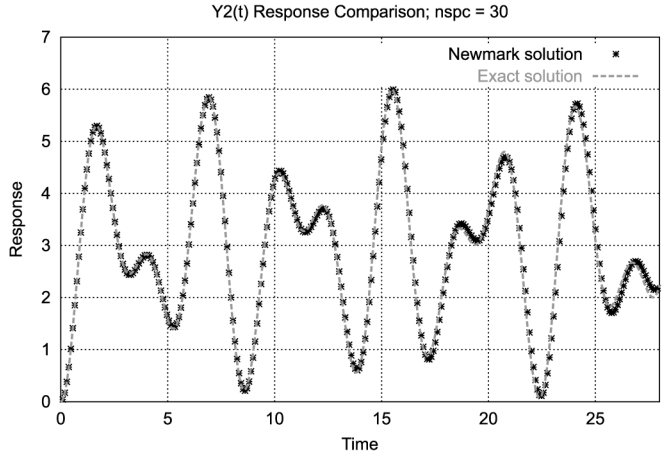

Figure 2.

particularly when one considers how cheap the structural equations are to solve compared to the fluid.

3. Aerodynamic model

A finite-volume Euler code is used for the aerodynamic model. The two-dimensional unsteady Euler equations on a moving grid in integral form are:

$$\frac{\partial}{\partial t}\iint_V \mathbf{U}\,\mathrm{d}x\,\mathrm{d}y + \int_{\partial V} \mathbf{F}\cdot\mathbf{n}\,\mathrm{d}S = 0 \tag{12}$$

where $\mathbf{U}$ is the vector of conserved variables, $\mathbf{F}$ is the flux vector, $\mathbf{n}$ is the outward cell face unit normal, and S the peripheral length of the cell face. $\mathbf{U}$ and $\mathbf{F}$ are given by:

$$\mathbf{U} = \begin{Bmatrix} \rho \\ \rho u \\ \rho v \\ \rho e \end{Bmatrix}, \qquad \mathbf{F} = \begin{Bmatrix} \rho(\mathbf{u} - \mathbf{X_t}) \\ \rho u(\mathbf{u} - \mathbf{X_t}) + P\mathbf{i} \\ \rho v(\mathbf{u} - \mathbf{X_t}) + P\mathbf{j} \\ \rho e(\mathbf{u} - \mathbf{X_t}) + P\mathbf{u} \end{Bmatrix} \tag{13}$$

where $\mathbf{u}$ is the velocity vector, $\mathbf{X_t}$ the grid velocity vector, and P, ρ, u, v and e are pressure, density, Cartesian x- and y-component velocities and total specific energy, respectively. The equation set is closed by

$$P = (\gamma - 1)\left(\rho e - \frac{\rho \mathbf{u}^2}{2}\right) \tag{14}$$

3.1 Discretisation

The unsteady Euler equations are solved using a Jameson (Jameson *et al.*, 1981) type cell-centred finite-volume method. Equation (12) is applied to each cell of the mesh. Following Jameson *et al.* (1981), the spatial and time dependent terms are decoupled and a set of ordinary differential equations are obtained. Artificial dissipation needs to be added to stabilise the solution (Jameson *et al.*, 1981; Kroll and Jain, 1987).

3.2 Aerodynamic time integration

It is expensive to use explicit time-stepping for unsteady flows. To maintain time-accuracy the whole domain must be integrated by the same time-step, and this is limited to the smallest value over the domain. Hence, an implicit scheme is used, based on that proposed by Jameson (1991). This solves the unsteady flows as a series of pseudo-steady cases, and is extremely efficient compared to an explicit scheme (Allen, 1997b; Gaitonde, 1994). Equation (1) is approximated for each computational cell at time level $(n+1)$ by

$$\frac{\mathrm{d}(V^{n+1}\mathbf{U}^{n+1})}{\mathrm{d}t} + \mathbf{R}^{n+1} = 0 \tag{15}$$

where V is the cell area, $\mathbf{R}$ is the flux integral, and the superscript $(n+1)$ denotes the time level $(n+1)\Delta t$. The $\mathrm{d}/\mathrm{d}t$ operator is approximated by an implicit second-order backward difference to give

$$\frac{3V^{n+1}\mathbf{U}^{n+1} - 4V^{n}\mathbf{U}^{n} + V^{n-1}\mathbf{U}^{n-1}}{2\Delta t} + \mathbf{R}(\mathbf{U}^{n+1}) = 0 \tag{16}$$

or

$$\mathbf{R}^{*}(\mathbf{U}^{n+1}) = \mathbf{R}(\mathbf{U}^{n+1}) + \frac{3V^{n+1}\mathbf{U}^{n+1} - 4V^{n}\mathbf{U}^{n} + V^{\mathrm{n}-1}\mathbf{U}^{n-1}}{2\Delta t} = 0 \tag{17}$$

To solve this $\mathbf{U}^{n+1}$ must be iterated upon until equation (17) $\rightarrow 0$. Hence, a fictitious derivative with respect to "pseudo time" τ can be introduced to the equation to give

$$V^{n+1}\frac{\mathrm{d}\mathbf{U}}{\mathrm{d}\tau} + \mathbf{R}^{*}(\mathbf{U}) = 0 \tag{18}$$

and the solution of equation (17) is then equivalent to marching equation (18) to a steady state in pseudo time, i.e. when $\mathbf{U}$ has been found such that $\mathrm{d}\mathbf{U}/\mathrm{d}\tau \rightarrow 0$ then $\mathbf{U}^{n+1} = \mathbf{U}$. There is no limit on the real time-step allowed, and steady acceleration techniques can be used in pseudo time. Equation (18) is solved using a multi-stage Runge-Kutta method with local time-stepping.

3.3 Moving mesh algorithm

The flow-solver is used in conjunction with a structured moving mesh, which allows the cell volumes to distort as the aerofoil moves or deforms. An algebraic moving grid generator based on transfinite interpolation (Eriksson, 1982; Gordon and Hall, 1973; Gordon and Thiel, 1982) is used. This approach is extremely efficient, as it allows instantaneous grid positions and speeds to be computed directly at any time (Allen, 1995, 1997a; Gaitonde and Fiddes, 1993).

The cell areas required in the time-stepping scheme can be calculated exactly in terms of the coordinates of the grid nodes. However, if the areas are calculated in this manner, errors will be introduced by the moving mesh. In order to avoid such errors, a geometric conservation law needs to be satisfied numerically, in addition to the mass, momentum and energy conservation laws that govern the physics of the flow (Thomas and Lombard, 1979). The areas must be integrated forward using the same numerical scheme as for the flow.

Figure 3 shows an example of a moving C-grid generated by the present method. A sequence of grids is shown for NACA 64A010 aerofoil pitching up 20°.

More details of the flow-solver can be found in the works Djayapertapa (2001) and Djayapertapa and Allen (2001).

4. Aero-structural coupling

There are two options when coupling separate aerodynamic and structural dynamic codes. The simplest method to couple separate aerodynamic and structural dynamic codes is "weak" coupling, wherein there is no intermediate

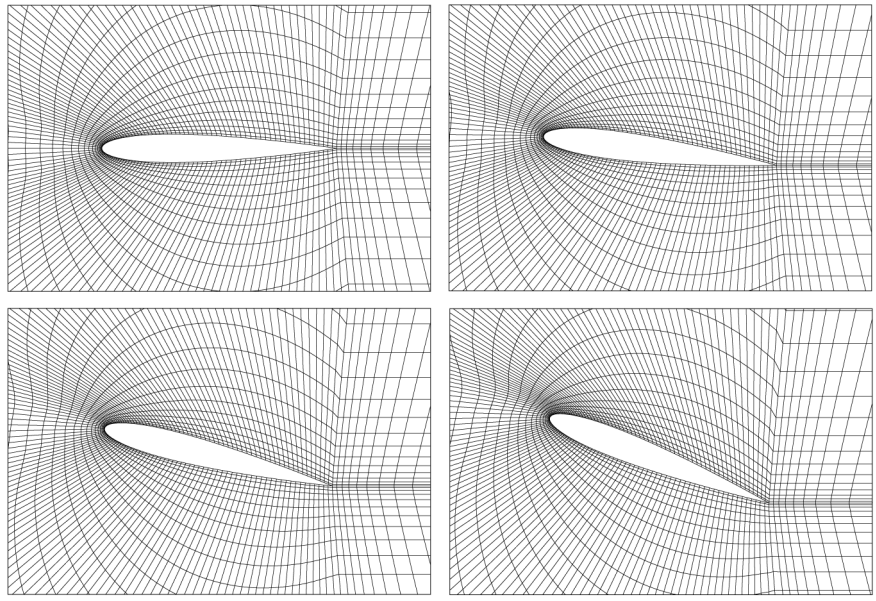

Figure 3.
Moving C-grid, NACA0012 aerofoil

exchange of information between the two solvers at each time level. At each time level the fluid is solved using the current structural position to give aerodynamic loads on the structure, and these are then used to solve for a new structural position. This is simply repeated for each time level. Hence, the fluid and structure are not synchronised in time, and there is always a phase lag between the two. This phase lag will be time-step dependent, and this has been examined earlier.

Alternatively "strong" coupling can be used, wherein there is exchange of information between the two solvers. At each real time level the aerodynamic loads are computed, then the structural position that results from those loads are computed. The aerodynamic loads around this new structural position are then recomputed, and this iterative procedure is repeated until the fluid and structure are perfectly synchronised at each real time level. This is more complex to code than weak coupling, but ensures there is no phase lag between fluid and structure. A flight control system is integrated with the aero-structural code in the next section, and it is clearly desirable that no phase lag is present in this case.

In fact, earlier it has been shown (Djayapertapa and Allen, 2001) that only for low numbers of real time-steps per period is the strong coupling scheme more expensive, in terms of CPU requirements, than the weak coupling scheme. However, in this region the phase lag is such that weak coupling is not of acceptable accuracy. As a flight control system is to be integrated which cannot function with inherent phase lag, the strong coupling scheme was chosen.

It has also been shown (Djayapertapa and Allen, 2001) that computations performed on a grid of density 147×32 points, using 60 real time-steps per cycle gave acceptable accuracy. Increasing either grid density or number of time-steps gave only small increases in accuracy, which were far outweighed by the increased computational cost.

4.1 Energy considerations

During an unsteady coupled calculation there will be energy transfer from fluid to structure, and vice versa, and it is useful to examine this energy transfer. The general energy identity (derivable from Lagrange's equation) is given by

$$E_{\text{total}} = \text{KE} + \text{PE} = E_{\text{o}} + W_{\text{ext}} \tag{19}$$

where E_{total} is the total mechanical energy of the structure, consisting of kinetic energy (KE) and potential energy (PE). E_{o} is the initial energy of the structure, i.e. the energy that the structure has at time $= 0$, and W_{ext} is the work done by external forces such as the aerodynamic forces.

$W_{\text{ext}} > 0$ indicates that work is being done by the fluid. If the amplitude of the structural oscillation grows then W_{ext} and E_{total} will also grow, but following the energy identity given by equation (19), the difference between the total energy and the work done by the aerodynamic forces should be constant. That identity can also be used to check the time integration scheme used. If the

difference is constant then no amplitude error or period elongation are introduced by the time integration scheme.

4.2 Computed responses for Isogai model

A two degree of freedom test case due to Isogai (1979) was first considered. The aeroelastic parameters used are

$$a_h = -2.0, \quad x_\alpha = 1.8, \quad r_\alpha = 1.87, \quad \frac{\omega_h}{\omega_\alpha} = 1.0, \quad \mu = 60. \tag{20}$$

This represents a typical section of a swept back wing, since the elastic axis is ahead of the leading edge.

Aeroelastic responses for plunge and pitch for speed index, U^*, values of 0.30, 0.5025 and 0.70 at a Mach number of 0.85 are shown in Figure 4. At the lower value of speed index the responses are decayed. These decayed responses are produced because the structural stiffness overpowers the work done by the fluids. As U^* increases the response reaches a neutrally stable condition in which the structural stiffness is just sufficient to dissipate the extracted energy – this is termed the flutter point (0.5025 in this case). When the speed index is increased further, the extracted energy overpowers the structural stiffness, hence diverging responses are obtained. The character of this divergent response then can be benign, i.e. small amplitude flutter or catastrophic, i.e. explosive flutter. The analysis of this character should be based on Hopf bifurcation or stability/instability of the LCO. For panel flutter, this analysis was performed by Librescu (1965, 1967), where the flutter character was termed "undangerous" or "dangerous", and was determined by the sign of the first Liapounov magnitude (Bautin, 1949).

Figure 5 displays the energy variations for the above three cases. The energy is non-dimensionalised by the initial energy E_0, so that the difference of the total energy and the work done by external forces should be equal to 1 as time increases. From Figure 5 we see that this difference remains constant and equal to the initial energy E_0, thus proving that the numerical scheme used is energy conserving.

The flutter point is located for a particular Mach number by computing the time-response for several values of speed index, and analysing the rate of decay for each one. When the speed index is found at which the rate of decay is zero, this is the flutter speed index at that Mach number. If the process of locating the flutter point is repeated for several Mach numbers the flutter boundary of the aerofoil can be computed. Therefore, it should be noted that the coupled code is not a "prediction" tool, but a simulation tool which, if required, can be used in a brute force way to compute flutter boundaries. The computed flutter boundary is shown in Figure 6, which also shows results due to Alonso and Jameson (1994), Isogai (1979) and Kousen and Bendiksen (1994). The results compare well.

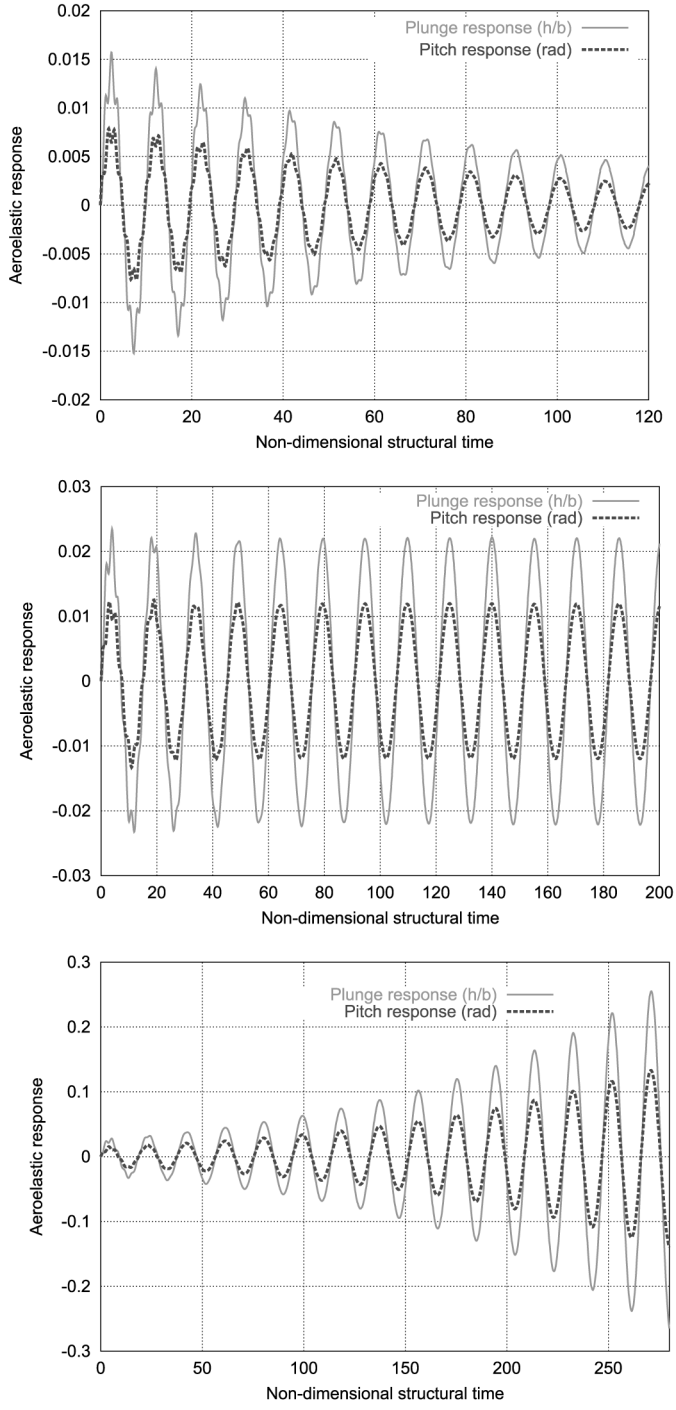

Figure 4.
Aeroelastic response, $U^* = 0.30$, 0.5025, 0.7, and Mach = 0.85

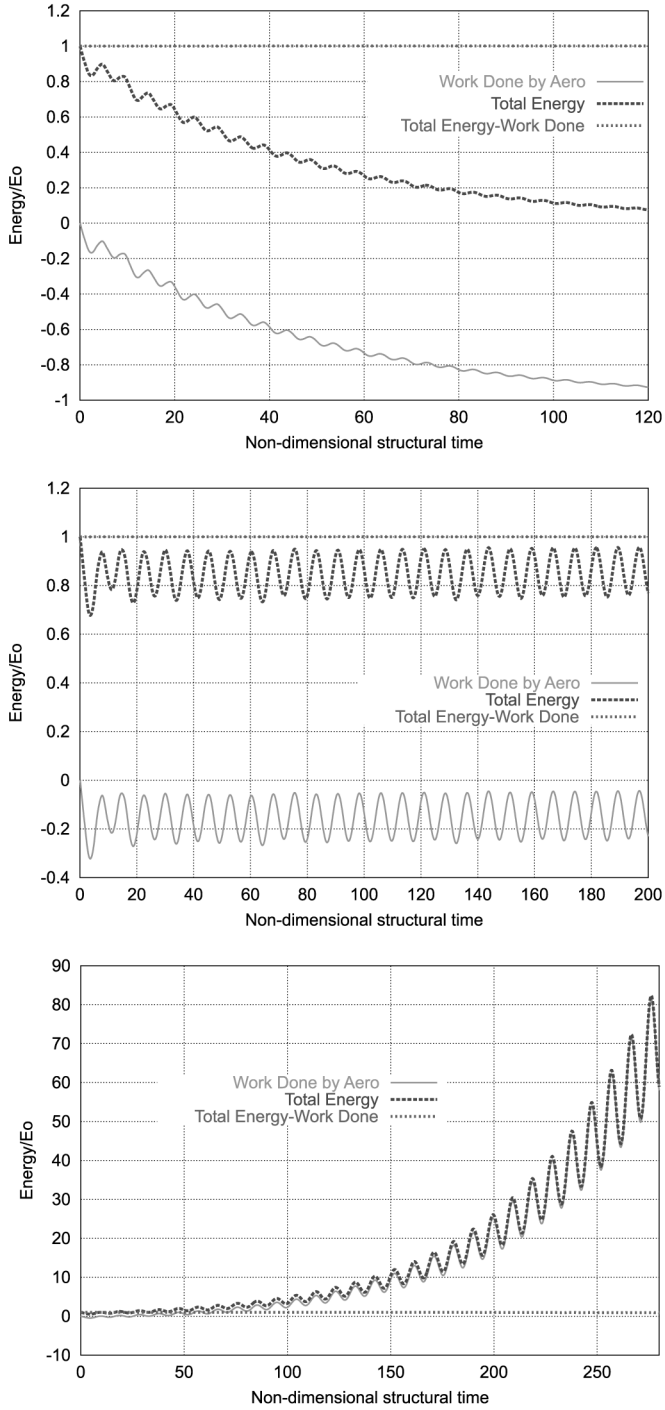

Figure 5.
Energy variations, $U^* = 0.30$, 0.5025, 0.7, and Mach = 0.85

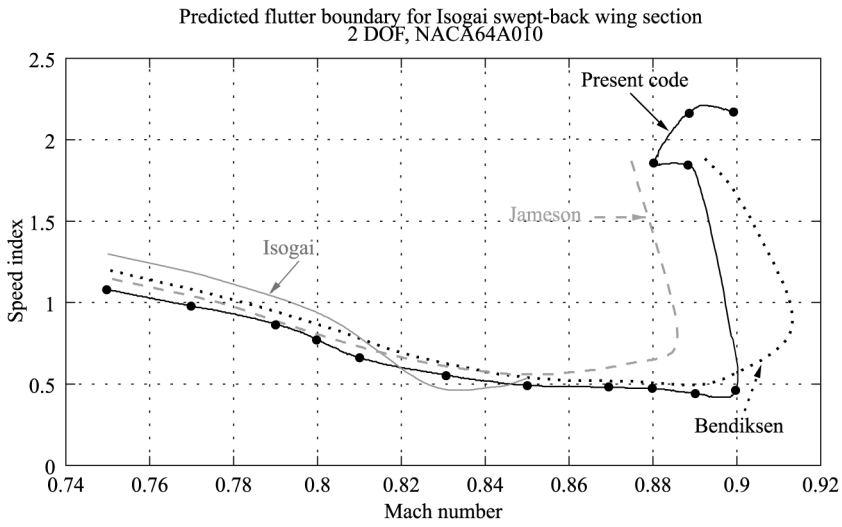

Figure 6.
Isogai model predicted flutter boundary

One interesting point to consider is the phase difference between the plunge and pitch motion. Figure 7 shows the phase difference for varying Mach number and speed index. This shows that in the lower transonic region the plunge and pitch motion are in phase even far above the flutter point. As the Mach number and speed index increase, this difference increases almost linearly, until there is a rapid change to antiphase motion at high Mach number. It is believed that once the Mach number becomes high enough, or the amplitude of oscillation becomes large enough (i.e. the speed index becomes large enough), the shockwaves on one or both sides will move to the trailing edge. Once this occurs the motion of the shocks becomes limited, and hence the section motion must change since the applied aerodynamic load variation changes.

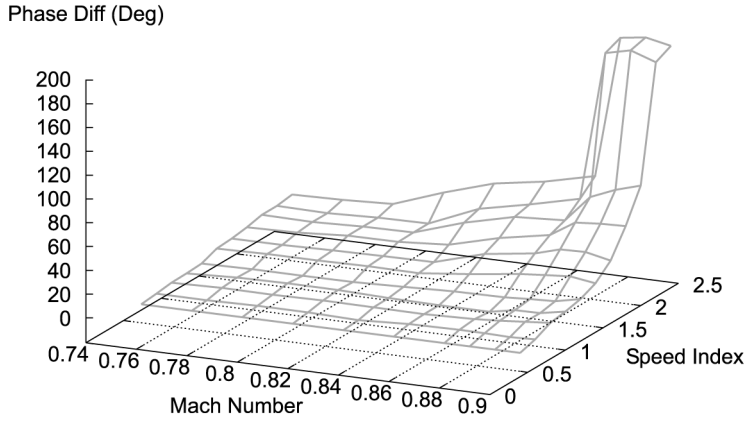

Figure 7.
Phase difference plot, Isogai model

4.3 Computed three degree of freedom response

A three degree of freedom was added to the NACA64A010 case used earlier. The structural parameters used for the calculations are as follows (Schulze, 1998):

$$a_h = -0.2, \quad x_\alpha = 0.2, \quad r_\alpha = 0.5, \quad \frac{\omega_h}{\omega_\alpha} = 0.3, \quad \mu = 23.48,$$

$$x_\beta = 0.008, \quad r_\beta = 0.06, \quad \frac{\omega_\beta}{\omega_\alpha} = 1.5, \quad C_\beta = 0.5 \tag{21}$$

The computed flutter boundary of the aerofoil is shown in Figure 8. The figure also shows results obtained by DLR (Schulze, 1998), and the two flutter boundaries compare very well.

5. Aeroservoelastic coupling

The trailing edge flap may be moved according to the instantaneous aerofoil state to attempt to reduce the structural deformation. Hence, active control has been implemented within the aeroelastic solver, in order to investigate active means of transonic flutter suppression via control surface (flap) and motion-aeroservoelasticity (closed loop calculations). A simple control law is used which relates the required flap deflection angle, β_c, to the motion of the main aerofoil surface (plunge and pitch degrees of freedom). Hence, β_c is evaluated according to the following equation

$$\beta_c = G_1\xi + G_2\alpha + G_3\dot{\xi} + G_4\dot{\alpha} + G_5\ddot{\xi} + G_6\ddot{\alpha} \tag{22}$$

where the G's are the gains of the system.

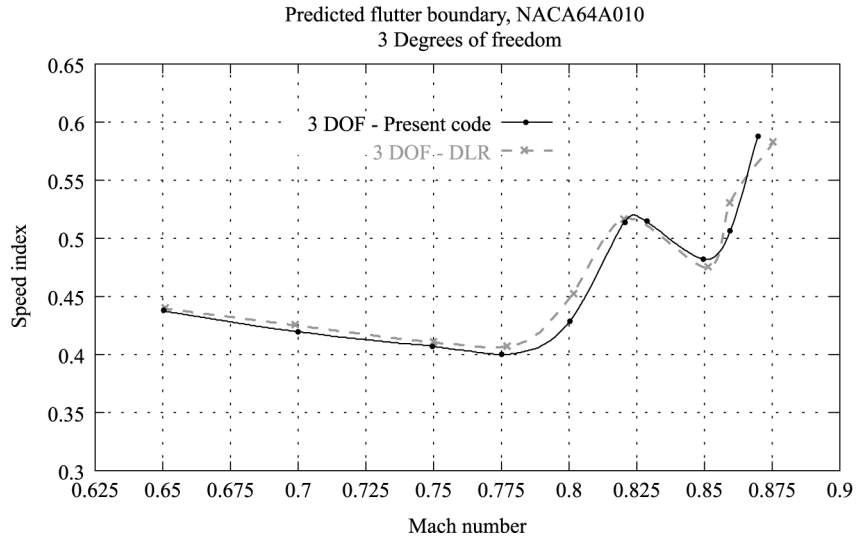

Figure 8.
Predicted flutter boundary for three degrees of freedom

The flap is moved according to the demanded deflection angle β_c. However, instead of moving the flap by β_c degrees within a certain amount of time (according to the flap deflection rate), the required angle is converted into equivalent control hinge moment (CHM) which is blended into the open loop aeroelastic equations as the external moment acting on the hinge axis, hence only affecting the β degree of freedom. There are two hinge moments on the right hand side of the aeroservoelastic equation, the aerodynamic hinge moment (AHM) and the CHM as shown by equation (23)

$$x_\beta \ddot{\xi} + \left[(C_\beta - a_h)x_\beta + r_\beta^2\right]\ddot{\alpha} + r_\beta^2\ddot{\beta} + \frac{4M_\infty^2\gamma}{U^{*2}\mu} r_\beta^2 \left(\frac{\omega_\beta}{\omega_\alpha}\right)^2 \beta = \underbrace{\frac{8M_\infty^2\gamma}{\pi\mu} C_{\mathrm{H}}}_{\mathrm{AHM}} + \underbrace{\frac{4M_\infty^2\gamma}{U^{*2}\mu} r_\beta^2 \left(\frac{\omega_\beta}{\omega_\alpha}\right)^2 \beta_c}_{\mathrm{CHM}} \tag{23}$$

This is because it is impossible to guarantee that the flap will move from β to $\beta + \beta_c$ within a certain amount of time. By converting the required angle to the equivalent CHM the flap dynamics are accounted for. Furthermore, from the open loop three degree of freedom case, it was seen that the flap motion also influences the pitch and plunge motion. That influence has already been included when the CHM was blended into the open loop aeroelastic equation.

The same time marching scheme is used to integrate the aeroservoelastic equation of motion, the only change lies in the representation of the right hand side force. It is now given by $\mathbf{f} = \mathbf{f_a} + \mathbf{f_c}$ where $\mathbf{f_c}$ is the control forces and is given by $\mathbf{f_c} = \{0, 0, \mathrm{CHM}\}^{\mathrm{T}}$.

The energy identity given by equation (19) should still hold, and the work done by external forces includes an extra term due to the control surface.

5.1 Computed closed loop responses

Closed loop simulations were performed using the active control. A Mach number of 0.85 was chosen, and the speed index was 5 per cent above the flutter speed, i.e. corresponding to an unstable response.

Different gain combinations were first considered in order to determine the optimum gain combinations to be used. From a series of calculations it was found that G_1, G_2, G_5 and G_6 fail to suppress the flutter, whereas G_3 and G_4 successfully suppressed the motion. The most effective combination was to use G_3 and G_4 together. Figure 9 shows the plunge, pitch and flap responses for $M = 0.85$, and $U^* = 1.05U^*_{\mathrm{flutter}}$. The initial disturbance was $\dot{\xi} = \dot{\alpha} = 0.01$ and the gains were $G_3 = G_4 = 1.0$. Two situations were considered: implementing the active control immediately, and at some later time. It is clear that the active control has managed to "drain" the

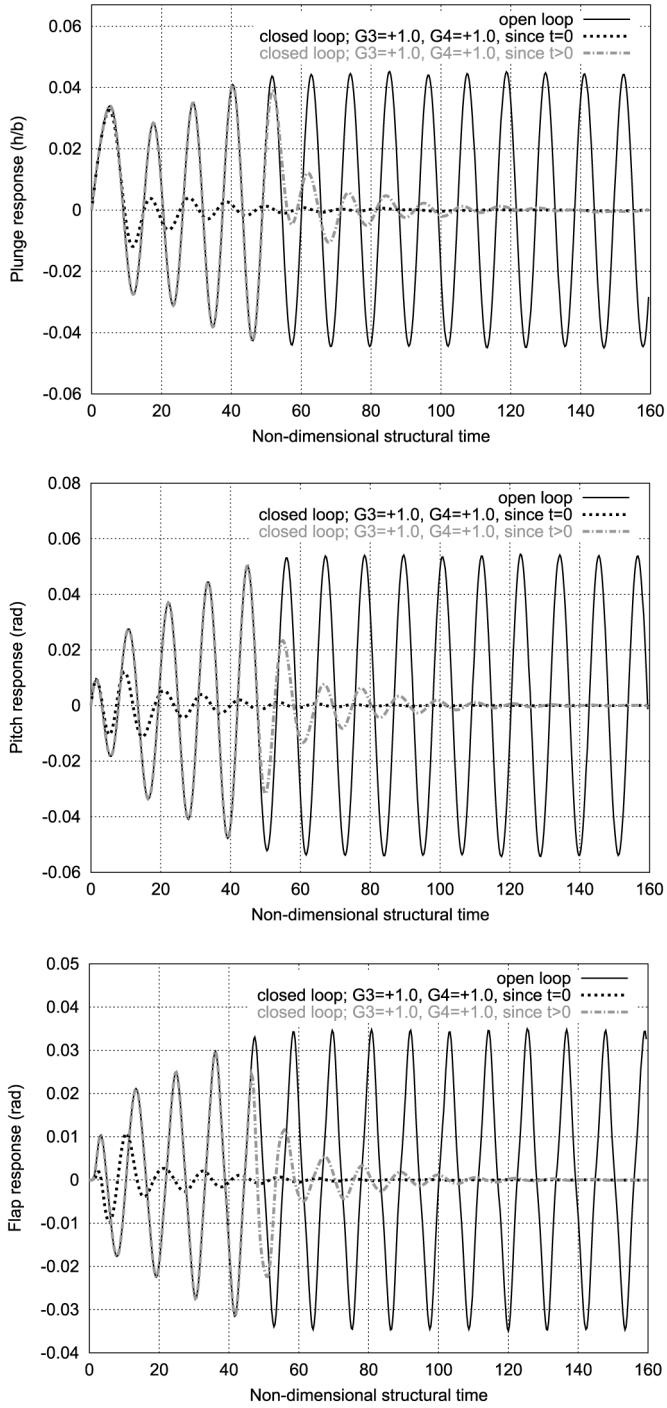

Figure 9.
Positive velocity feedback; $G_3 = +1.0$, $G_4 = +1.0$, and $U^* = 1.05\ U_f^*$

structural energy very quickly, even when the disturbance has sufficient time to grow.

The effect of the control law on the flutter boundary was then considered. The open and closed loop flutter boundaries are shown in Figure 10. The control law works very effectively within the transonic region, where the shock position can be affected by the flap. An increase of upto 19 per cent in the allowable speed index can be achieved with this control law.

The mechanics of transonic flutter and active control were investigated by considering a more unstable case. Figure 11 shows a series of flowfield Mach contours for $M = 0.85$, and $U^* = 1.10U^*_{\text{flutter}}$ without active control. The same aerofoil was used, but the grid density was increased to 211×40 to capture the shock more sharply. Contours are plotted every quarter period, for six periods. These show how the out of phase shock motion across the flap causes the oscillation to grow. Figure 12 shows Mach contours for the same case with active control switched on just before the end of the third cycle. The flap is clearly effective in controlling the shock motion in this case.

It should be remembered that an inviscid aerodynamic model is used here, and that viscous effects are likely to be significant for this type of flow, where there are shock waves present and a moving control surface.

5.2 Effect of sampling frequency

A real flight control system would sample the aerofoil state continuously, whereas it is only sampled at discrete points in time here. Hence, the effect of time-step size on the active control was considered. The above computations were performed with 60 real time-steps per period. The above case was run again with 240 time-steps per period. Figure 13 shows the plunge, pitch, and

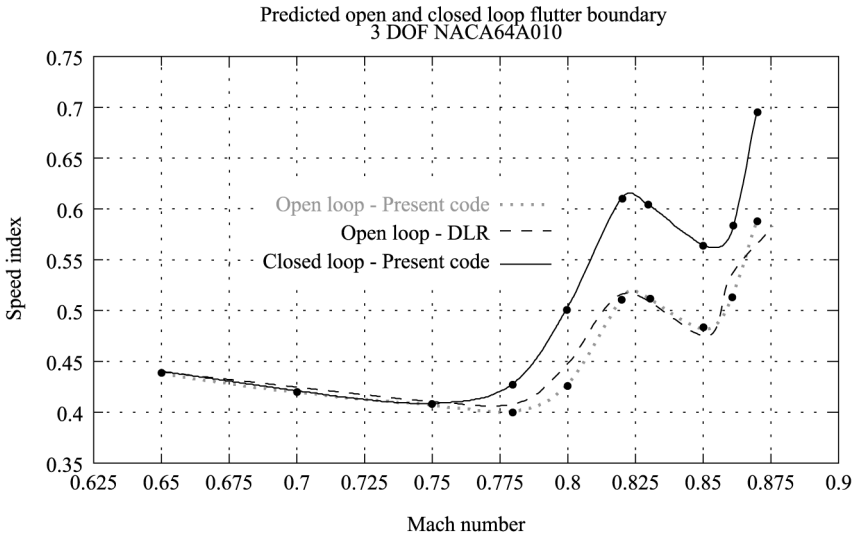

Figure 10.
Control law effectiveness

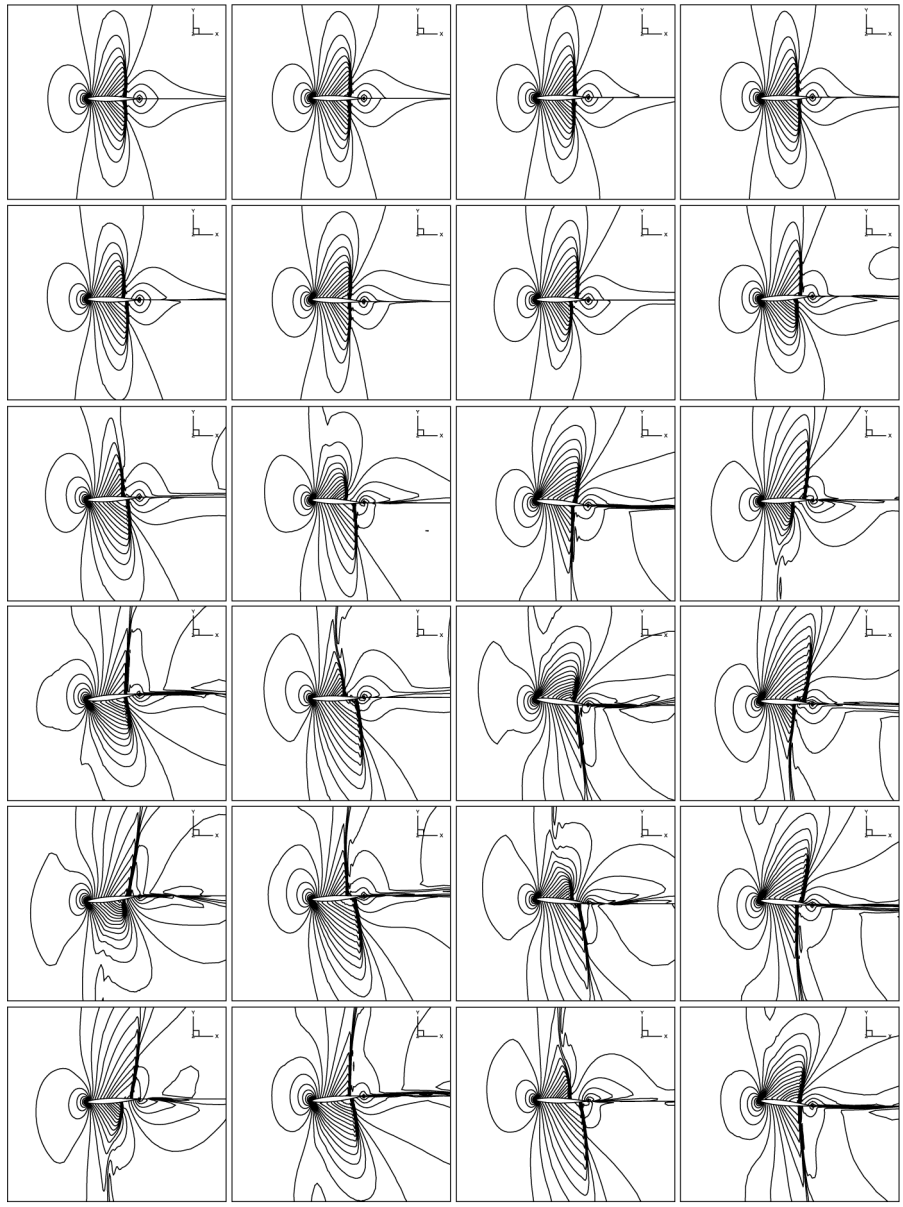

Figure 11.
Open loop flowfield mach contours

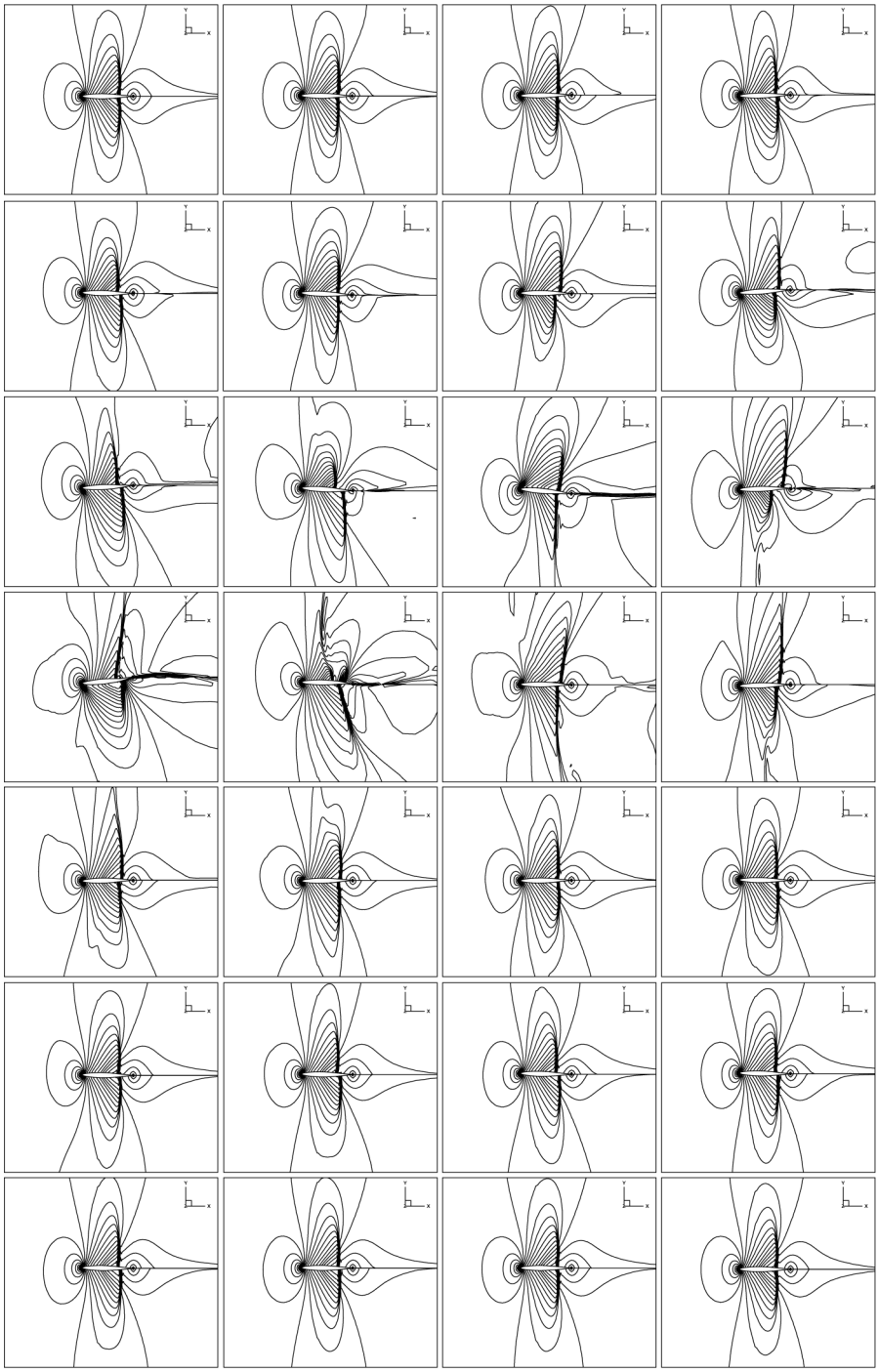

Figure 12.
Closed loop flowfield mach contours

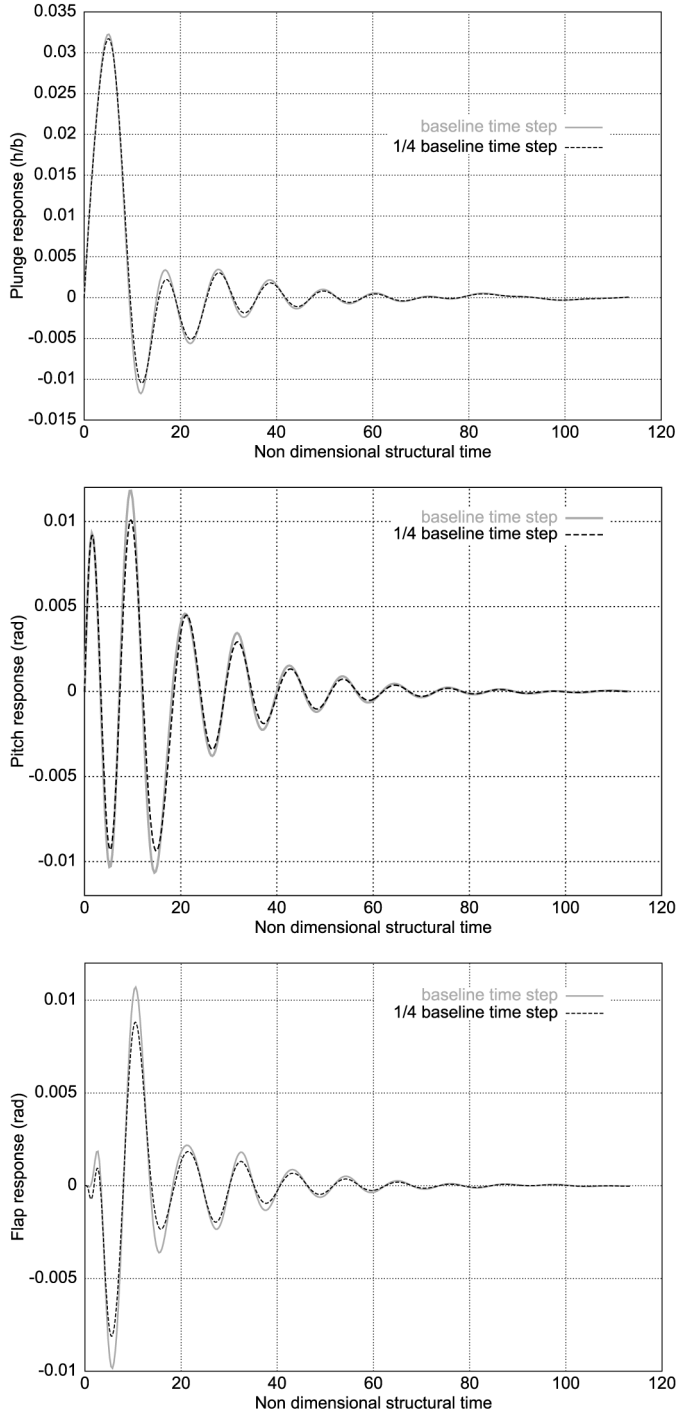

Figure 13.
Effect of reducing the real time-step size

flap variations for the two sampling frequencies. It is clear that there is very little difference between the two cases.

6. Non-linear structural model

The effect of structural non-linearity on aeroservoelastic calculations has also been considered. Backlash (free-play) in the torsional spring of the control surface motion was considered.

Figure 14 plots the variation of the hinge moment against the flap deflection angle. The solid line represents the linear variation that has been used so far, and the dashed line shows the typical non-linear characteristics for backlash. There is a range of rotational amplitude where the restoring hinge moment is zero, outside this range a linear relationship between the restoring hinge moment and flap deflection angle exists.

Free-play of the hinge axis modifies the aeroelastic and aeroservoelastic equation only for the β (flap) degree of freedom. Outside the free-play region the equation of motion for the flap degree of freedom is given by

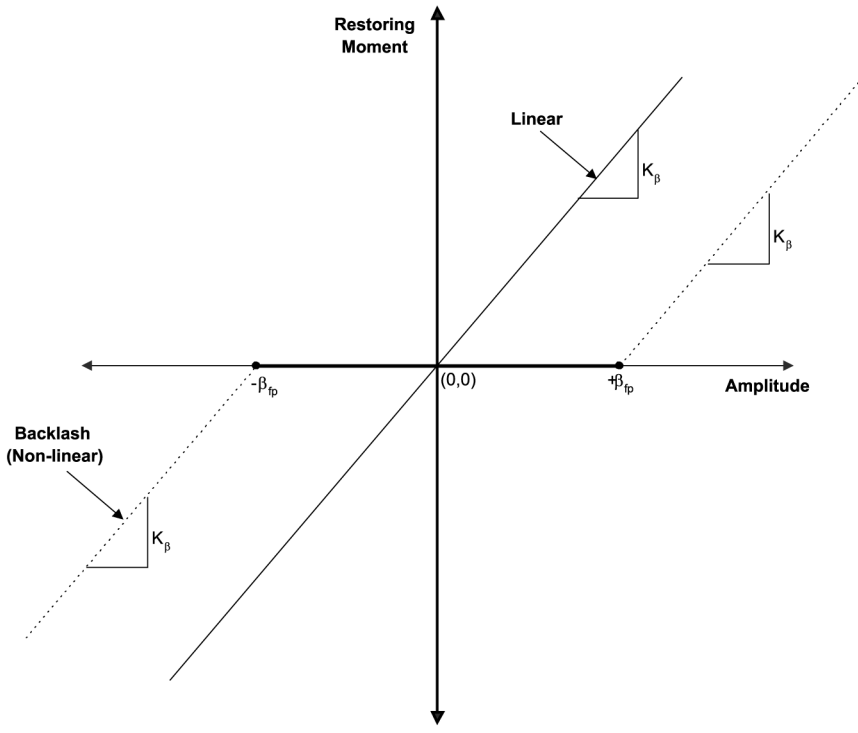

Figure 14.
Linear and non-linear moment relation

$$x_\beta \ddot{\xi} + \left[(C_\beta - a_h)x_\beta + r_\beta^2\right]\ddot{\alpha} + r_\beta^2 \ddot{\beta} + \frac{4M_\infty^2 \gamma}{U^{*2}\mu} r_\beta^2 \left(\frac{\omega_\beta}{\omega_\alpha}\right)^2 \beta = \underbrace{\frac{8M_\infty^2 \gamma}{\pi\mu} C_H}_{\text{AHM}} + \underbrace{\frac{4M_\infty^2 \gamma}{U^{*2}\mu} r_\beta^2 \left(\frac{\omega_\beta}{\omega_\alpha}\right)^2 \beta_c}_{\text{CHM}} \pm \underbrace{\frac{4M_\infty^2 \gamma}{U^{*2}\mu} r_\beta^2 \left(\frac{\omega_\beta}{\omega_\alpha}\right)^2 \beta_{\text{fp}}}_{\text{FPHM}} \quad (24)$$

where the positive sign is used when $\beta > \beta_{\text{fp}}$ and negative sign is used when $\beta < -\beta_{\text{fp}}$ to evaluate free-play hinge moment (FPHM). The same time-marching scheme can be used again to integrate equation (24), as only change lies in the representation of the right hand side force. It is now given by $\mathbf{f} = \mathbf{f_a} + \mathbf{f_c} + \mathbf{f_{fp}}$ where $\mathbf{f_{fp}}$ is the free play hinge moment and is given by $\mathbf{f_{fp}} = \{0, 0, \text{FPHM}\}^{\text{T}}$.

As before the energy identity given by equation (19) should still hold. The work done by the external forces includes an extra term when β is outside the free-play region. Inside the free-play region this term and the control surface term are both zero.

6.1 Computed responses

Open and closed loop calculations were performed for the three degree of freedom case presented above, now with the non-linear CHM. The aerofoil is the NACA64A010 section, the Mach number is 0.85 and the flutter speed index was chosen. The effects of the free-play of 1.0° in the hinge axis torsional spring on the aeroelastic responses are shown in Figure 15. From the figure it can be seen that free-play actually causes the responses to grow and settle into a limit cycle oscillation, i.e. the effect is destabilising.

Results for active control calculations with backlash are shown in Figure 15. It can be seen that the responses are damped when the required flap angle β_c falls outside the free-play area. However, once the response has settled, and β_c lies within the free-play area, there is not much that the control law can do, since it is utilising the CHM to suppress the motions, and within the free-play area the control hinge moment is zero. From the plot of energy it is clear that the control law drains the energy until β_c falls within the free-play area.

Figure 16 shows the open loop phase plane plots for plunge, pitch and flap deflection for the linear structural model and free-play of one degree. Figure 17 shows flap deflection phase plane plots for closed loop calculations with and without free-play. With free-play the flap settles into a periodic motion.

It should also be noted here that the effect of signal sampling frequency, i.e. size of the real time-step used, was also considered in the free-play region.

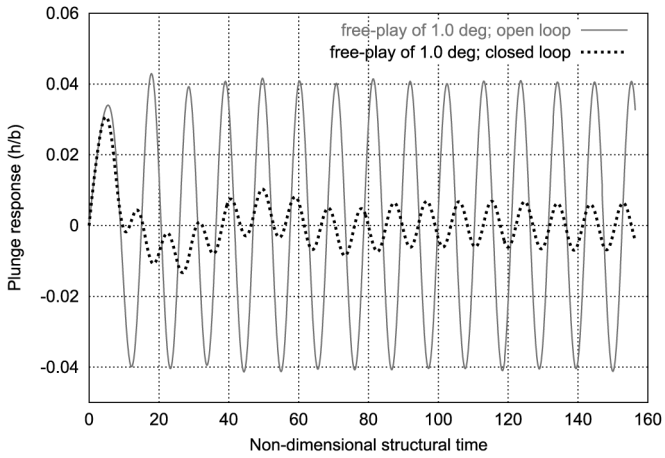

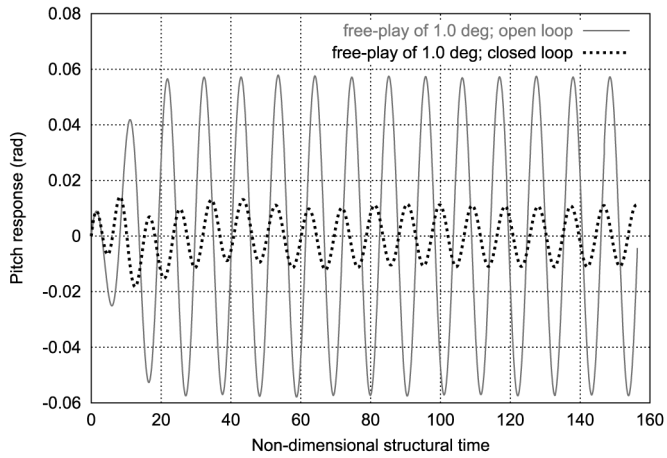

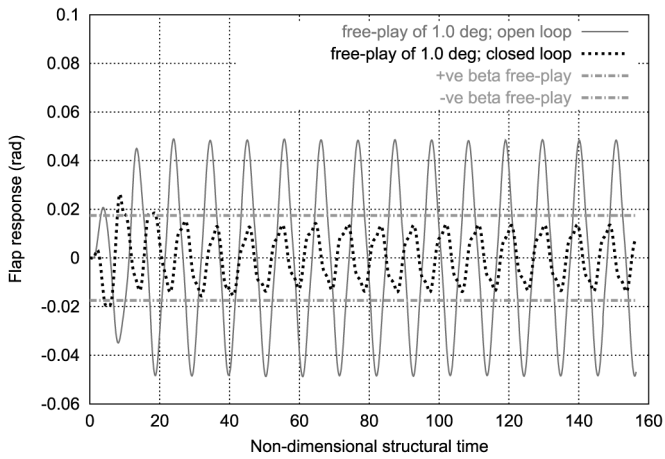

(*continued*)

Figure 15.
The effects of free-play of 1.0 deg

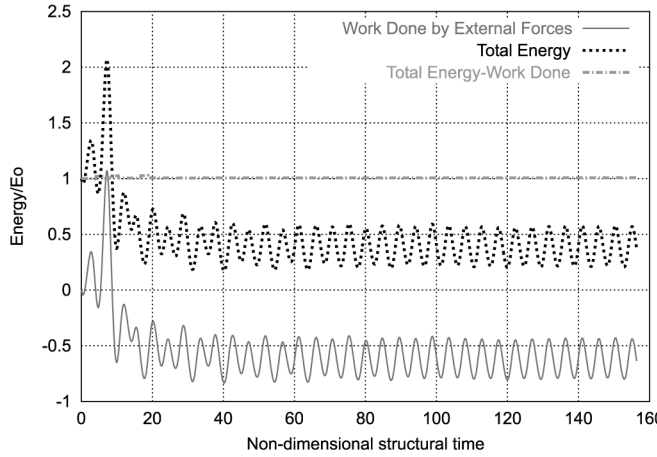

Figure 15.

Again there was only a small amplitude dependence on the time-step size, and no frequency dependence, as in Section 5.2.

7. Conclusions

Numerical simulations of transonic flutter and active control have been performed, by coupling independent aerodynamic and structural dynamic codes in the time domain. A simple control system has also been integrated with the coupled code, and since this requires perfect synchronisation of fluid, structure and control signal, the "strong" approach to coupling has been adopted. Two and three degree of freedom two-dimensional structural models have been considered. The consistency of the coupling has been demonstrated by considering the total energy of the structure and work done by the fluid. The difference between the two remains constant with time regardless of the structural motion.

The coupled scheme has been used to simulate time responses to structural disturbances for various Mach numbers and speed indices, to attempt to compute flutter boundaries for the two and three degree of freedom cases, and the results compare well with other published data. Furthermore, the structural model has been extended to include an actively controlled trailing edge flap, and this has succesfully been used to increase the stability margin by means of control surface motion. The aerofoil velocity feedback signal was found to give the best suppression results, and for the NACA64A010 aerofoil an increase of up to 19 per cent in the allowable speed index can be achieved within the transonic region. Furthermore, it has been shown that active control is still effective when there is free-play in the control hinge – the aerofoil response is supressed to within the free-play region.

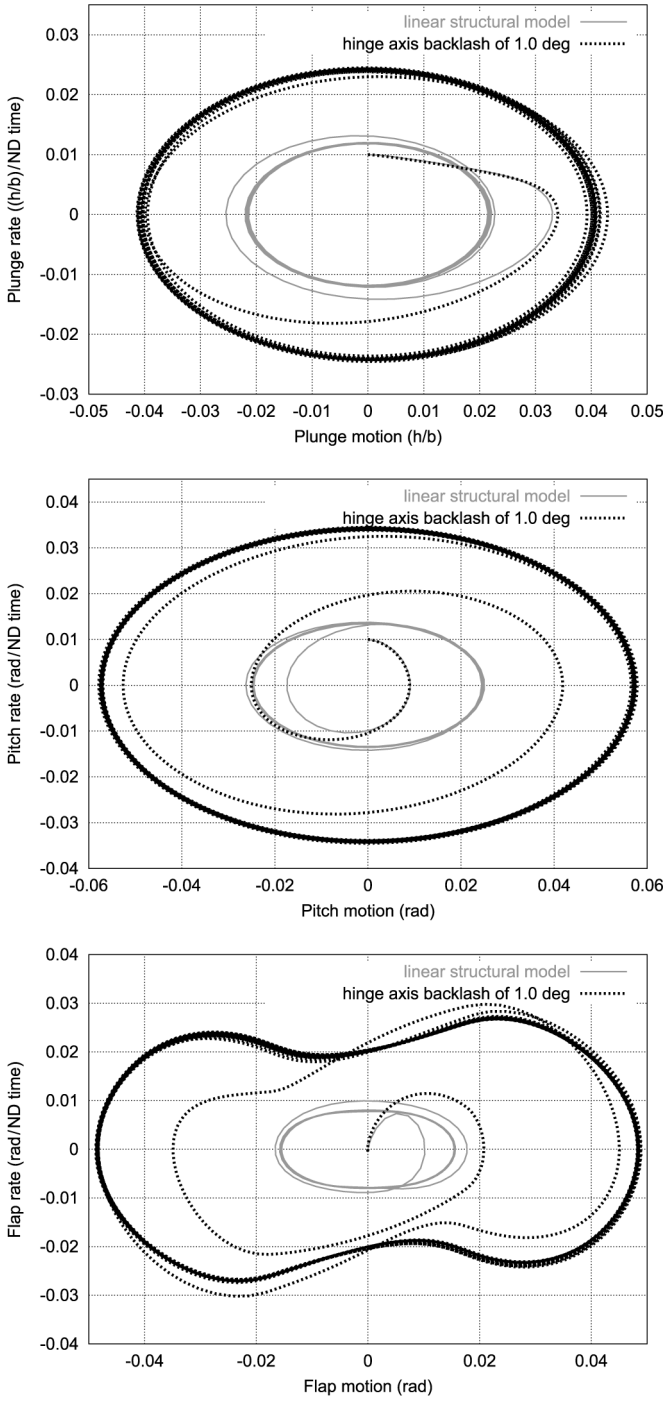

Figure 16.
Phase plane plots for linear and non-linear structure

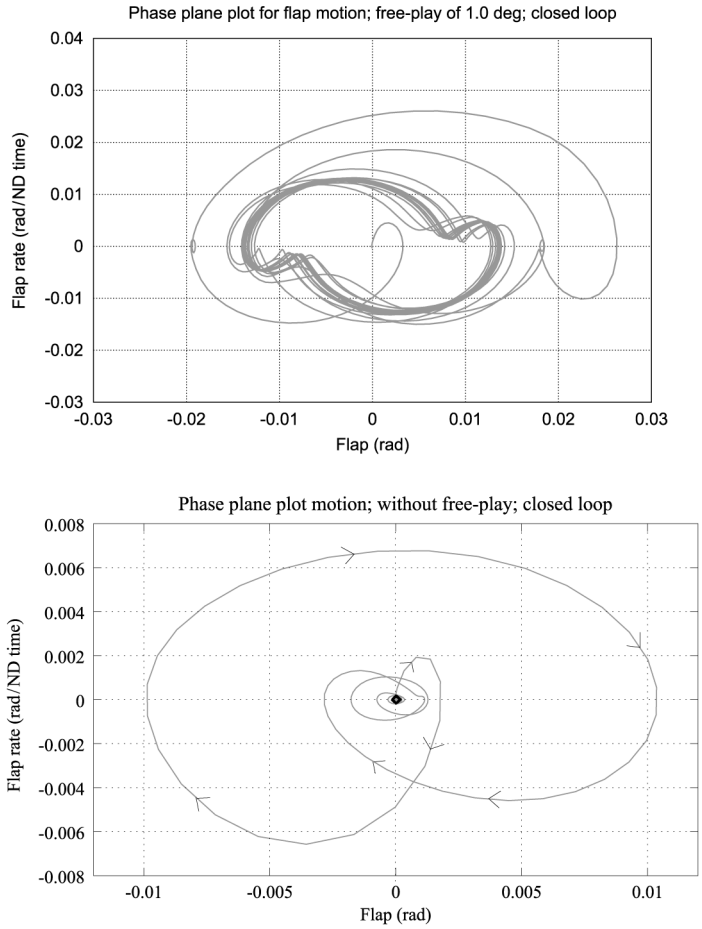

Figure 17.
Closed loop flap phase plane comparison with and without free-play

The mechanics of transonic flutter and active control have been examined by considering time-dependent flowfield data, and the fundamental importance of shock wave motion has been clearly demonstrated.

References

Allen, C.B. (1995), "Central-difference and upwind biased schemes for steady and unsteady Euler aerofoil flows", *Aeronautical Journal*, Vol. 99, pp. 52-62.

Allen, C.B. (1997a), "The reduction of numerical entropy generated by unsteady shockwaves", *Aeronautical Journal*, Vol. 101 No. 1001, pp. 9-16.

Allen, C.B. (1997b), "Grid adaptation for unsteady flow computations", *I. Mech. E. J. of Aerospace Eng.,* Part G4, Vol. 211, pp. 237-50.

Alonso, J.J. and Jameson, A. (1994), "Fully-implicit time-marching aeroelastic solutions", *AIAA Paper No. 94-0056*, Reno, NV.

Badcock, K.J., Sim, G. and Richards, B.E. (1995), "Aeroelastic studies using transonic flow CFD modelling", *Proceedings International Forum on Aeroelasticity and Structural Dynamics*, June 1995, Manchester, pp. 18.1-18.12.

Bathe, K.J. (1982), *Finite Element Procedures in Engineering Analysis*, Prentice-Hall, Englewood Cliffs, NJ.

Batina, J.T. and Yang, T.Y. (1984), "Application of transonic codes to aeroelastic modelling of airfoils including active controls", *Journal of Aircraft*, Vol. 21 No. 8, pp. 623-30.

Bautin, N.N. (1949), *Behaviours of Dynamic Systems in the Vicinity of the Boundary of the Stability Domain*, Gostekizdat, Moscow.

Bendiksen, O.O. and Kousen, K.A. (1987), "Transonic flutter analysis using the Euler equations", *AIAA Paper No. 87-0911-CP*, Reno, NV.

Bennett, R.M. and Edwards, J.W. (1998), "An overview of recent development in computational aeroelasticity", *AIAA 98-2421, 29th AIAA Fluid Dynamics Conference*, Albuquerque, NM.

Bland, S.R. and Edwards, J.W. (1984), "Airfoil shape and thickness effects on transonic airloads and flutter", *Journal of Aircraft*, Vol. 21, pp. 209-17.

Djayapertapa, L. (2001), "A computational method for coupled aerodynamic-structural calculations in unsteady transonic flow with active control study", PhD thesis, Aerospace Engineering Department, Bristol University.

Djayapertapa, L. and Allen, C.B. (2001), "Time-marching analysis of aeroservoelasticity", *Paper 1, Proceedings RAeS Aerodynamics Conference*, London.

Dowell, E.H., *et al.* (Eds) (1994), *A Modern Course in Aeroelasticity*, 3rd revision and enlarged edition, Kluwer Academic Publishers, Boston, MA.

Edwards, J.W., Breakwell, J.V. and Bryon, A.E. Jr (1978), "Active flutter control using generalized unsteady aerodynamic theory", *Journal of Guidance and Control*, Vol. 1 No. 1, pp. 32-40.

Eriksson, L.E. (1982), "Generation of boundary conforming grids around wing-body configurations using transfinite interpolation", *AIAA Journal*, Vol. 20 No. 10, pp. 1313-20.

Försching, H. (1995), "Challenges and perspectives in computational aeroelasticity", *Proceedings International Forum on Aeroelasticity and Structural Dynamics*, June 1995, Manchester, pp. 11.1-11.9.

Fung, Y.C. (1955), *An Introduction To the Theory of Aeroelasticity*, Wiley, New York, NY.

Gaitonde, A.L. (1994), "A dual-time method for the solution of the unsteady Euler equations", *The Aeronautical Journal*, Vol. 98, pp. 283-91.

Gaitonde, A.L. and Fiddes, S.P. (1993), "A three dimensional moving mesh method for the calculations of unsteady transonic flows", *Paper 13 in Proceedings of the 1993 European Forum for Recent Developments and Applications in Aeronautical CFD*, Bristol.

Glaser, J. (1987), *Seminar on Aeroelasticity*, de Havilland, Canada.

Gordon, W.J. and Hall, C.A. (1973), "Construction of curvilinear co-ordinates systems and applications to mesh generation", *International Journal for Numerical Methods in Engineering*, Vol. 7, pp. 461-77.

Gordon, W.J. and Thiel, L.C. (1982), "Transfinite mappings and their application to grid generation", in Thompson, J.F. (Ed.), *Numerical Grid Generation*, North Holland.

Guillot, D. and Friedman, P.P. (1994), "A fundamental aeroservoelastic study combining unsteady CFD with adaptive control", *AIAA 94-1721*, Reno, NV.

Guillot, D. and Friedman, P.P. (1995), "Adaptive control of aeroelastic instabilities in transonic flow using CFD based loads", *Proceedings International Forum on Aeroelasticity and Structural Dynamics*, June 1995, Manchester, pp. 73.1-73.13.

Guruswamy, G.P. (1989a), "Integrated approach for active coupling of structures and fluids", *AIAA Journal*, Vol. 27 No. 6, pp. 788-93.

Guruswamy, G.P. (1990), "Unsteady aerodynamic and aeroelastic calculations for wings using Euler equations", *AIAA Journal*, Vol. 28 No. 3, pp. 461-9.

Guruswamy, G.P. and Tu, E.L. (1989b), "Transonic aeroelasticity of fighter wings with active control surfaces", *Journal of Aircraft*, Vol. 26 No. 7, pp. 682-4.

Horikawa, H. and Dowell, E.A. (1979), "An elementary explanation of the flutter mechanism with active feedback controls", *Journal of Aircraft*, Vol. 16 No. 4, pp. 225-32.

Isogai, K. (1979), "On the transonic-dip mechanism of flutter of a sweptback wing", *AIAA Journal*, Vol. 17 No. 7, pp. 793-5.

Jameson, A. (1991), "Time dependent calculations using multigrid, with applications to unsteady flows past airfoils and wings", *AIAA Paper 91-1596*, Reno, NV.

Jameson, A., Schmidt, W. and Turkel, E. (1981), "Numerical solutions of the Euler equations by finite volume methods using Runge-Kutta time stepping schemes", *AIAA-Paper No. 81-1259*, Reno, NV.

Karpel, M. (1982), "Design for active flutter suppression and gust alleviation using state-space aeroelastic modelling", *Journal of Aircraft*, Vol. 19 No. 3, pp. 221-7.

Kousen, K.A. and Bendiksen, O.O. (1988), "Non-linear aspects of the transonic aeroelastic stability problem", *AIAA Paper No. 88-2306, AIAA/ASME/ASCE/AHS 29th Structures, Structural Dynamics and Material Conference*, Denver, CO.

Kousen, K.A. and Bendiksen, O.O. (1994), "Limit cycle phenomena in computational transonic aeroelasticity", *Journal of Aircarft*, Vol. 31 No. 6, pp. 1257-63.

Kroll, N. and Jain, R.K. (1987), "Solution of two dimensional Euler equations – experience with a finite volume code", *DLR Report, DFVLR-FB 87-41*.

Librescu, L. (1965), "Aeroelastic stability of orthotropic heterogeneous thin panels in the vicinity of the flutter critical boundary (I)", *Journal de Mecanique*, Vol. 4 No. 1, pp. 51-76.

Librescu, L. (1967), "Aeroelastic stability of orthotropic heterogeneous thin panels in the vicinity of the flutter critical boundary (II)", *Journal de Mecanique*, Vol. 6 No. 1, pp. 133-52.

MacNeal Schwendler Corporation (1995), "MSC/NASTRAN aeroelastic analysis", *Seminar Notes Version 68*.

Meijer, J.J., Hounjet, M.H.L., Eussen, B.J.G. and Prananta, B.B. (1998), "NLR-TU Delft experience in unsteady aerodynamics and aeroelastic simulation applications", *AGARD Report No. 822, Numerical Unsteady Aerodynamic and Aeroelastic Simulation*, pp. 11.1-11.21.

Nissim, E. (1971), "Flutter suppression using active controls based on the concept of aerodynamic energy", *NASA TN D-6199*.

Nissim, E. (1977), "Recent advances in aerodynamic energy concept for flutter suppression and gust alleviation using active controls", *NASA TN D-8519*.

Nissim, E. (1990), "Design of control laws for flutter suppression based on the aerodynamic energy concept and comparisons with other design methods", *NASA TP 3056*.

Nissim, E. and Abel, I. (1978), "Development and application of an optimization procedure for flutter suppression using the aerodynamic energy concept", *NASA TP 1137*.

Nissim, E., Caspi, A. and Lottatti, I. (1978), "Application of the aerodynamic energy concept to flutter suppression and gust alleviation by use of active controls", *NASA TP 1137*.

Noll, T.E. (1993), "Aeroservoelasticity", in Noor, A.K. and Venneri, S.L. (Eds), *Flight-Vehicle Materials, Structures, and Dynamics-Assessment and Future Direction, Structural Dynamics and Aeroelasticity*, Chapter 3. Vol. 5, pp. 179-212.

Pak, C.G., Friedman, P.P. and Livne, E. (1991), "Transonic adaptive flutter suppression using approximate unsteady time domain aerodynamics", *AIAA-91-0986-CP*, Reno, NV.

Prananta, B.B. and Hounjet, M.H.L. (1996), "Aeroelastic simulation with advanced CFD methods in 2D and 3D transonic flow", *Symposium Unsteady Aerodynamics 1996, RAeS*, 17-18 July, London, UK.

Prananta, B.B., Hounjet, M.H.L. and Zwaan, R.J. (1995), "Thin layer Navier-Stokes solver and its application for aeroelastic analysis of an airfoil in transonic flow", *Proceedings International Forum on Aeroelasticity and Structural Dynamics*, June 1995, Manchester, pp. 1.1-1.9.

Robinson, B.A., Batina, J.T. and Yang, H.T.Y. (1991), "Aeroelastic analysis of wings using the Euler equations with s deforming mesh", *Journal of Aircraft*, Vol. 28 No. 11, pp. 781-8.

Scanlan, R.H. and Rosenbaum, R. (1951), *Introduction to the study of Aircraft Vibration and Flutter*, Macmillan, New York, NY.

Schulze, S. (1998), "Transonic aeroelastic simulation of a flexible wing section", *AGARD Report No. 822, Numerical Unsteady Aerodynamic and Aeroelastic Simulation*, pp. 10.1-11.20.

Schuster, D.M., Beran, P.S. and Huttsell, L.J. (1998), "Application of the ENS3DAE Euler/Navier-Stokes aeroelastic method", *AGARD Report No. 822, Numerical Unsteady Aerodynamic and Aeroelastic Simulation*, pp. 3.1-3.11.

Thomas, P.D. and Lombard, C.K. (1979), "Geometric conservation laws and its application to flow computations on moving grid", *AIAA Journal*, Vol. 17 No. 10, pp. 1030-7.

Whalley, R. and Ebrahimi, M. (1998), "Vibration and control of aircraft wings", *Proceedings of IMechE,* Part G, Vol. 212, pp. 353-65.